Ibn Al-Haitham Journal for Pure and Applied Sciences
Journal homepage: jih.uobaghdad.edu.iq
PISSN: 1609-4042, EISSN: 2521-3407
IHJPAS. 2026; 39(1)

CrIII, MnII and CoII Complexes with Schiff Base Ligand; Synthesis, Characterization, Physicochemical and Thermal Properties

Mohammed Qays Mezher[1] and **Enaam Ismail Yousif**[2*]
[1,2]Department of Chemistry, College of Education for Pure Science (Ibn Al-Haitham), University of Baghdad, Baghdad, Iraq
*Corresponding Author

Received: 24/May/2025
Accepted: 11/August/2025
Published: 20/ January /2026
doi.org/10.30526/39.1.4210

Abstract

Synthesis and characterization of a Schiff base ligand (HL), derived from ((E)-3-((4-acetylphenyl)diazenyl)-2-hydroxy-1-naphthaldehyde) with 1-amino-4-nitrobenzene in a one-to-one molar ratio. This study aims to synthesize and characterize HL. Subsequently, the interaction of ligand with different metal ions involving chromium (III), manganese (II) and cobalt (II) in the ratio of one ligand to one metal, resulted in the isolation of tetra and hexa-coordinate monomeric compound have been fully characterized using analytical methods and spectroscopic methods involve elemental microanalysis, ^{1}H and ^{13}C (NMR), (FT-IR) spectroscopy, as well as electronic spectra and magnetic moment magnetic susceptibility along with mass spectroscopy, in addition, thermal analysis and conductivity measurements. The FTIR analysis showed the presence of functional groups, including carbonyl, imine, and azo, as well as vibrations (M-OH$_2$), (M-O), (M-N), and (M-Cl). Mass spectrometry identified a deprotonated molecular ion ([M-H]$^+$) for the ligand at m/z= 437.55 amu (1%). The electron spectra and magnetic moments: 3.80, 5.91, 4.66 BM for chromium, manganese, and cobalt complexes, respectively. It has been proposed that the chromium and manganese complexes adopt distorted octahedral geometries, whereas the cobalt complex adopts a tetrahedral geometry.

Keywords: 1-Amino-4-nitrobenzene, ((E)-3-((4-Acetylphenyl)diazenyl)-2-hydroxy-1-naphthaldehyde), Metal complexes, Proteus mirailis, Schiff base ligand.

1. Introduction

The class of nitrogen-containing organic compounds possesses a general structure 'R-CH=N-R', called a Schiff base, ('R) and (R') may represent alkyl or aryl groups[1–3]. Schiff bases, characterised by the azomethine group (–C=N–), are synthesised by the reaction of primary amines along with reactive carbonyl molecules, including aldehydes or ketones. Schiff bases constitute a notable family of molecules in medical and pharmaceutical chemistry, possessing several biological uses, including antibacterial properties[4–6], antifungal activity[7], and antitumor activity. Antitumor agents have garnered considerable interest in the biological field because of their promising medicinal uses, including anti-inflammatory, antibacterial, cytotoxic, and antiviral[8–11]. They serve as catalysts, intermediates in organic synthesis, and stabilizers for polymers[12]. The effective use of Schiff-base π-systems in display devices is enhanced by their ability to impose a specific geometric architecture and to affect the electrical structure. Establish the excellent stability of the related coordination compounds and their improved solubility in standard organic solvents. These ligands, including nitrogen- and oxygen-donor atoms, serve as effective chelating agents for both transition and non-transition metals, forming stable complexes with most transition metals[13–15]. As pharmaceutical agents, Schiff base metal complexes have promise[16–19]. They can readily bind to metal ions and establish stable complexes. These complexes are highly regarded for their many applications across various fields[20]. In recent years, we have documented the production of Schiff base chemicals and the complexes they create[21–23]. This study deals with the formation of molecules containing a Schiff base. Examining the coordination properties of HL when interacting with metal ions is another goal of this effort. The synthesis of the ligand, including the preparation of (E)-3-((4-acetylphenyl)diazenyl)-2-hydroxy-1-naphthaldehyde, with 1-amino-4-nitrobenzene, generated the Schiff base ligand (HL). Furthermore, the interaction of HL with the chromium (III), manganese (II), and also cobalt (II) ions led to the isolation of some paramagnetic coordination compounds. This study also investigated the physicochemical and thermal properties of these synthesized chemicals.

2. Materials and Methods

2.1. Materials and procedures for experimentation

This study used a Bruker 400 MHz spectrometer to obtain NMR spectra of the ligand (^{1}H and ^{13}C) in DMSO-d_6 solutions, using TMS as the reference (400 MHz for ^{1}H and 100 MHz for ^{13}C) at Tehran University, the Islamic Republic of Iran. FTIR spectroscopy was performed on an FTIR-600 infrared Fourier spectrometer, recording spectra from 4000 to 200 cm^{-1} with KBr granules at the University of Baghdad, College of Science. A Sciex ESI mass spectrometer was employed for positive ion electrospray mass spectrometry at Tehran University, the Islamic Republic of Iran. A Stuart SMP4 electrothermal apparatus was used to determine the melting points in the Department of Chemistry, College of Education for Pure Science (Ibn Al-Haitham), University of Baghdad. UV-visible spectra were obtained using a Shimadzu UV-160A spectrophotometer within the 200–1000 nm range. The spectra were obtained from 10^{-3} mol L^{-1} solutions in dimethyl sulfoxide (DMSO), analysed at room temperature in a 1 cm quartz cuvette at the Department of Chemistry, College of Education for Pure Science (Ibn Al-Haitham), University of Baghdad. The conductivity of DMSO solutions was assessed at concentrations ranging from 10^{-1} to 10^{-5} M using an Eutech Instruments Cyber Scan CON 510 digital conductivity meter at the Department of Chemistry, College of Education for Pure Science (Ibn Al-Haitham), University of Baghdad. Elemental analysis for carbon, hydrogen, and nitrogen was conducted using a Heraeus Vario EL analyser, whilst metal content was assessed with a Shimadzu AA-7000 atomic absorption spectrometer at the Central Service Laboratory, University of Tehran, the Islamic Republic of Iran. The chloride ion concentration was determined using potentiometric titration employing a Metrohm 686 Titro processor and a 665 Dosim unit at Ibn Sina Company, Ministry of Industry, Iraq. Magnetic moments were measured using a Johnson Matthey magnetic susceptibility balance at Al-Mustansiriyah University, College of Science, Department of Chemistry. Thermogravimetric analysis–differential thermogravimetry (TGA-DTG) was conducted with an Instruments SDT Q600 V20.9 Build 20 at Beam Gostar Taban Laboratory, Islamic Republic of Iran.

2.2. Synthesis

2.2.1. Preparation of Schiff base ligand

Preparation of HL was based on the described process[24]. Initially, a mixture containing ((E)-3-((4-acetylphenyl)diazenyl)-2-hydroxy-1-naphthaldehyde) (1.0 g, 3.14 mmol), was dissolved in (20 mL) mixed solution (5:5) (ethanol-benzene). In comparison, the solution was stirred with the addition of 1-amino-4-nitrobenzene (0.433 g, 3.14 mmol) in 10 mL of ethanol, and 3 drops of glacial acetic acid were added. The reaction mixture was heated to 70-80°C and refluxed for 6 hours. The solution was filtered while still hot. The red precipitate had been filtered and washed with 5 mL of EtOH. The final product was dried in air; the ligand yield was 0.801 g (58.09%), with a melting point of 170-172°C.

2.2.2. Preparation of complexes

The synthesis of the complexes followed a similar procedure to that used to synthesise the Mn(II) complex. The procedure is as follows:

In a 100 mL round-bottom flask containing 0.3 g (0.68 mmol) of the Schiff base ligand, the ligand was dissolved in 10 mL of a mixed solvent (5:5) of ethanol and benzene. Five mL of an ethanolic KOH solution (0.038 g, 0.68 mmol) was then added to the solution. The reaction mixture was continuously stirred while $MnCl_2.6H_2O$ (0.13 g, 0.68 mmol) in ethanol (5 mL) was added dropwise. The reaction mixture was subsequently heated under reflux for two hours. After heating and filtering the solid, the residue was purified with cold ethanol and air-dried; the yield of the Mn (II) complex was 0.277 g (72.93%), which decomposed above 300°C. The synthesis process has been described in **Scheme 1**.

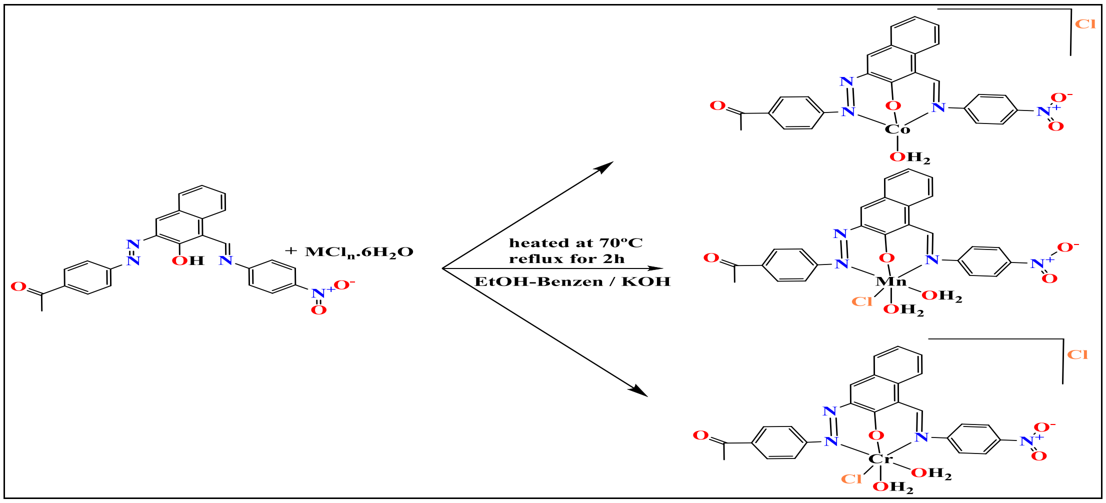

Scheme 1. General route for the synthesis of HL complexes

3. Results

The information on yields, colors, the quantity of metal salts utilized, and the m.p. of the resulting complexes is shown in **Table 1**. The proposed formula, molecular weight, and elemental microanalysis are shown in **Table 2**.

Table 1. Yield, colors and m.p. of compounds

Compound	Metal salt amount (g)	Complex amount (g)	Colour	M.p. (ºC)
$[Cr(L)Cl(H_2O)_2]Cl$	0. 18	0.40	Brown	229-231
$[Mn(L)Cl(H_2O)_2]$	0.13	0.38	Reddish-brown	>300*
$[Co(L)(H_2O)]Cl$	0.16	0.37	Dark brown	>300*

*=Decomposed

Table 2. Micro-analysis and physical characteristics of compounds

Compound	Molecular formula	M.Wt	Microanalysis (calculated)% found				
			C	H	N	M	Cl
$[Cr(L)Cl(H_2O)_2]Cl$	$C_{25}H_{21}C_{l2}CrN_4O_6$	596.36	(50.35) 50.04	(3.55) 3.33	(9.39) 9.10	(8.72) 8.40	(11.89) 11.55
$[Mn(L)Cl(H_2O)_2]$	$C_{25}H_{21}ClMnN_4O_6$	563.85	(53.25) 53.06	(3.75) 2.36	(9.94) 9.63	(9.74) 9.42	(6.29) 6.00
$[Co(L)(H_2O)]Cl$	$C_{25}H_{19}ClCoN_4O_5$	549.83	(54.61) 54.15	(3.48) 3.11	(10.19) 10.00	(10.72) 10.24	(6.45) 6.23

3.1. The FT-IR data

The FTIR of complexes displayed characteristic peaks for carbonyl, imine, and azo groups with additional bands related to the ν (M-OH$_2$), ν (M-O), ν (M-N), and ν (M-Cl). The information is shown in **Table 3**.

Table 3. The analysis of FT-IR for the most significant peaks (cm^{-1})

Complexes	ν(C= O) ν(C= N)	ν (C=C)	ν N=N	ν C -O ν C -N	$\nu(H_2O)$ $\nu(M-OH_2)$	ν (M -O) phenolic	ν M -N	ν M -Cl
$C_{25}H_{21}Cl_2CrN_4O_6$	1674 1614	1595 1548	1452	1361 1265	3334 754	634	487 430	275
$C_{25}H_{21}ClMnN_4O_6$	1674 1618	1597 1552 1502	1450	1357 1257	3414 756	630	489 420	264
$C_{25}H_{19}ClCoN_4O_5$	1678 1618	1539 1504	1475	1382 1263	3452 752	661	474 420	-

3.2. The NMR data

The ^1H NMR spectra of the ligand are depicted in **Figure 1**. Two distinct signal sets in the aromatic and aliphatic sections of the spectra. The chemical shift at δ 9.68 ppm corresponds to the phenolic proton. The aromatic region displayed many chemical alterations within the range of 9-6 ppm. The aliphatic region showed a singlet peak for the methyl group at 2.60 ppm. The spectra exhibited peaks at 2.51 and 3.37 ppm, corresponding to the DMSO-d_6 solvent and the amount of H_2O molecules in the solvent, respectively.

The ^{13}C-NMR spectrum of HL is illustrated in **Figure 2**. The spectra exhibited two separate sets of signals in the aromatic and aliphatic regions. This shows the correct number of carbon atoms in a molecule. Resonances at δc=197.11 and 177.23 ppm were assigned to carbonyl carbon: (ketonic); (iminic), respectively. The Signal of phenolic carbon was detected at 172.74 ppm. Aromatic ring carbons were observed at 150.10 to 109.62 ppm. The methyl group (C_i) appeared as a single peak at 27.15 ppm, while the solvent signals of DMSO-d_6 resonated at 40.17 ppm.

3.3. Mass spectrum

The ligand mass spectrum in **Figure 3** shows the presence of a parent ion $(M-H)^+$ at m/z=437.55 amu (1%), corresponding to $C_{25}H_{18}N_4O_4$.

3.4. Electronic spectra and magnetic moment

The electron spectra of the complexes show characteristic peaks between 257 and 298 nm, indicating $\pi\rightarrow\pi^*$ and $n\rightarrow\pi^*$ transitions. Further, charge-transfer phenomena account for the observed peaks in the array between 314 and 481 nm. Electronic spectra, magnetic moments, and molar conductivities for the complexes are given in **Table 4**.

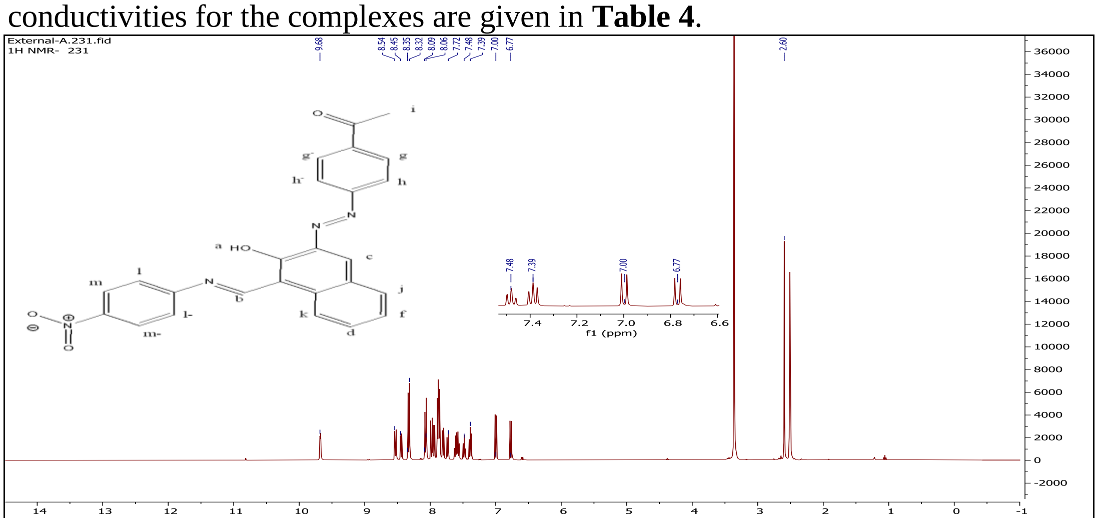

Figure 1. The ^1H-NMR spectrum of the ligand

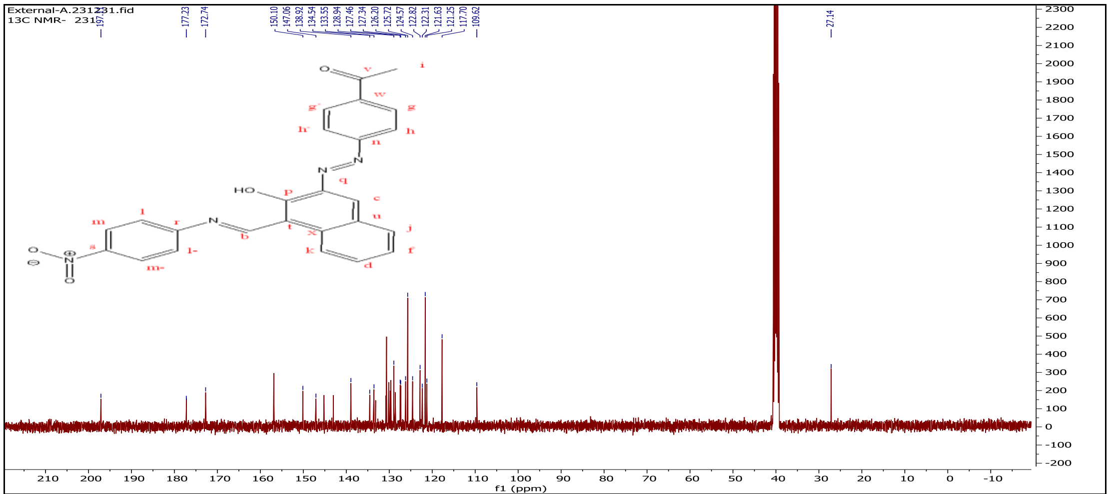

Figure 2. The ^{13}C-NMR spectrum of the ligand

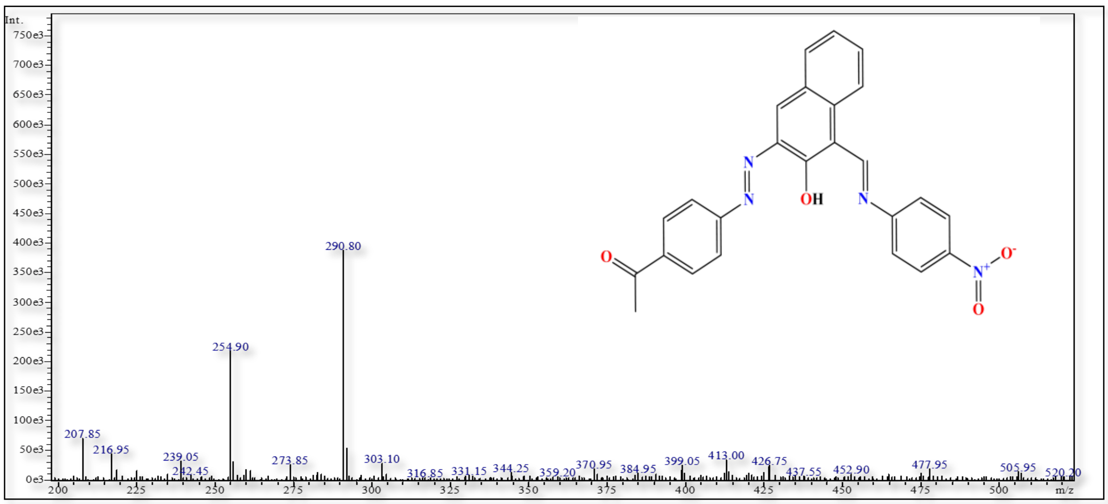

Figure 3. Mass spectrum of the ligand.

Table 4. Uv-vis, molar conductivity and magnetic moment for complexes

Compounds	ʎ (nm)	Molar extinction coefficient ε_{max} (dm^3 mol^{-1} cm^{-1})	Assignment	Λm $S.cm^2$. $mole^{-1}$	μ_eff	Suggested geometry
$[Cr(L)Cl(H_2O)_2]Cl$	292 397 486 697	1520 1450 1630 5	Intra-ligand $\pi \rightarrow \pi^*$, $n \rightarrow \pi^*$ C.T C.T $^4A_2g \rightarrow {}^4T_2g$	39.22	3.80	Distorted octahedral
$[Mn(L)Cl(H_2O)_2]$	226 318 374 460 611	1010 430 570 240 1	Intra-ligand $\pi \rightarrow \pi^*$, $n \rightarrow \pi^*$ C.T C.T C.T $^6A_{1g} \rightarrow {}^4E_g{}^{(D)}$	8.40	5.91	Distorted octahedral
$[Co(L)(H_2O)]Cl$	319 389 481 676	1680 1780 1190 2	Intra-ligand $\pi \rightarrow \pi^*$, $n \rightarrow \pi^*$ C.T C.T $^4A_2{}^{(F)} \rightarrow {}^4T_1{}_{(p)}$	48.57	4.66	Tetrahedral

3.5. Thermal analysis

The thermogravimetric analysis–difference thermogravimetry (TGA-DTG) curves for ligand and Cr (III) complex are shown in **Figures 4** and **5**, respectively. It explains the decomposition of compounds and the number of stages involved.

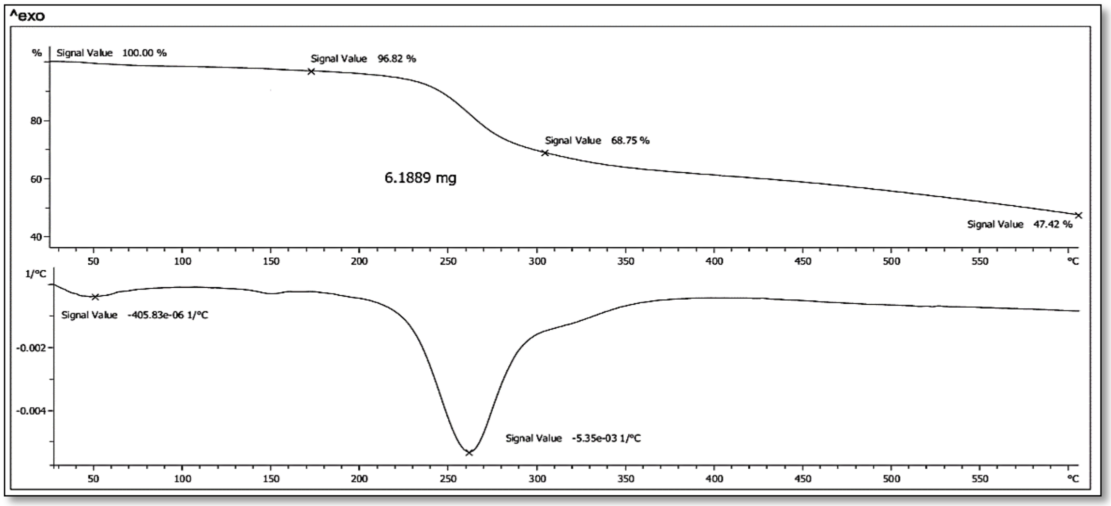

Figure 4. The thermal analysis curves of ligand in Ar atmosphere.

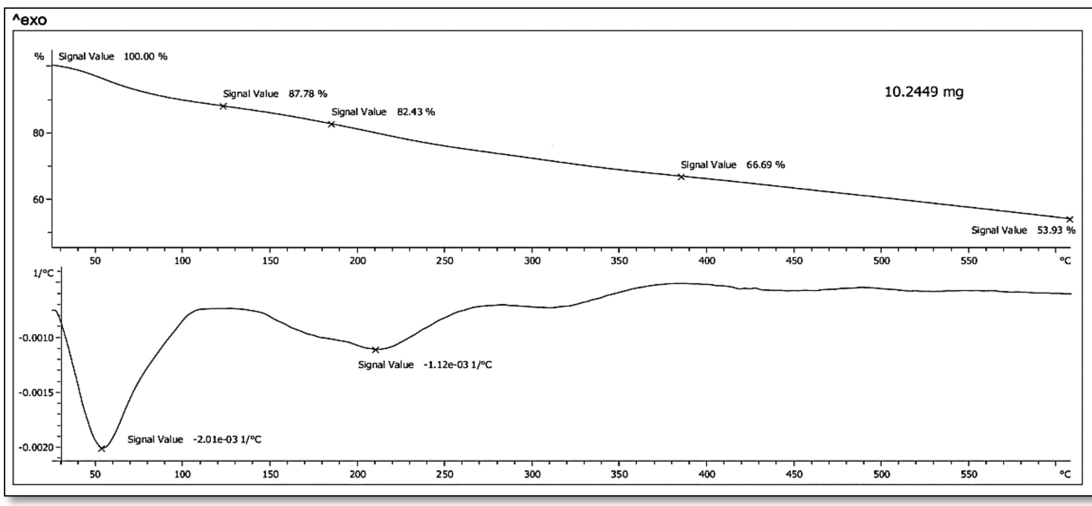

Figure 5. The thermal analysis curves of Cr (III) complex in Ar atmosphere.

4. Discussion

The Schiff base ligand (1-(4-((E)-(3-hydroxy-4-((E)-((4-nitrophenyl)imino) methyl) naphtha len-2-yl) diazenyl) phenyl) ethan-1-one)) (HL) formation from 1-amino-4-nitrobenzene with ((E)-3-((4-acetylphenyl)diazenyl)-2-hydroxy-1-naphthaldehyde) reacting in EtOH at a one-to-one ratio. The ligand functions as a tridentate species, donating the nitrogen atom, hydroxyl group, and nitrogen imine. The interaction of the HL along with the metals chlorides for Cr (III), Mn (II) and Co (II) in a one to one mole ratio (L:M), resulted in identification of tetra- and also hexa-coordinate monomeric compounds with the universal formula [M(L) Cl $(H_2O)_2$] Cl with chromium (III), [M(L) Cl $(H_2O)_2$] with Mn (II) and [M (L) H_2O] Cl with cobalt (II) ion, **Scheme 1**. The isolated compounds exhibited air stability, manifested as solid forms, and were reported to be soluble in DMSO and dimethylformamide. However, it is insoluble in other prevalent organic solvents. Based on their physicochemical data, the coordination geometries and complexation behavior of the complexes were inferred. The results shown in **Table 2** are well-suited to the proposed formula. Molar conductance measurements in DMSO solutions indicated that each of the complexes operates as an electrolyte, except the Mn complex, which exhibited nonelectrolyte behavior at a 1:1 ratio.

4.1. The FT-IR and NMR data

The primary IR spectral data for the complexes will be displayed in **Table 3**, along with their assignments. The peak is observable in the ligand spectra at 3408 cm^{-1}, which is attributable to the stretch of the phenol hydroxyl group, ν(OH). The bands appear at 1624 cm^{-1} and 1487 cm^{-1}, corresponding to the stretch of the imine group ν(C=N) and the azo group ν(N=N), respectively[26]. Complex spectra showed a noticeable band between 1618 cm^{-1} and 1614 cm^{-1}, attributed to ν(C=N). The interaction between a metal ion and the ν(C=N) imine moiety is elucidated by the bands that emerge during complexation[25]. The band reported at 1487 cm^{-1} in ligand, which belongs to the azo group, ν(N=N)[23,25]. It was displaced and appeared at 1475, 1454, and 1465 cm^{-1} in the three complexes, in that order. The occurrence might have been associated with the nitrogen atom's involvement in complexation. In addition, the metal complexes' spectra exhibited additional bands at (684-621) and (499-418) cm^{-1}, which weren't present in the ligand spectrum, related to ν(M-O), ν(M-N), and ν(M-Cl), respectively[25,26]. Finally, the complex spectra for Cr(III), Mn(II), and Co (II) exhibited peaks at 3452, 3412, and 3439 cm^{-1}, respectively, which were bound to aqua molecules, at 752, 746, and 742 cm^{-1}, complex bands 1, 2, and 3 can be found. These are linked to water-coordinated ν(M-OH)[26,27] for 1,2 and 4. The ^{1}H NMR of the ligand with DMSO (d_6) as a solvent is shown in **Figure 1**. The spectra exhibited two distinct categories of signals in the aromatic and aliphatic regions. The aromatic region displayed many chemical alterations within the range of 9-6 ppm. The chemical shift at δ 9.68 ppm (s, 1H) corresponds to the phenolic proton $H_{(a)}$. The chemical shift was exhibited as a singlet signal at 8.54; 8.45 ppm (s, 1H), which is equivalent to $H_{(b)}$ and $H_{(c)}$ protons, respectively. The spectrum shows a doublet signal for $H_{(g,g-)}$ at 8.35 (d, J = 9.1Hz, 2H). The signal reveals as a doublet at 8.32 (d, J=8.7Hz, 2H) attributed to $H_{(l,l-)}$ when the frequency value 8.09 (d, J=8.1Hz, 2H) belongs to $H_{(h,h-)}$ proton. The doublet signal attributed to H(m,m-) displays at 7.72 (d, J=7.9Hz, 2H). The value of $H_{(d)}$ appears as a triplet signal at 7.48 (t, J=7.5Hz, 1H). The value of $H_{(f)}$ appears as a triplet signal at 7.39 (t, J=7.5Hz, 1H), when another doublet signal is displayed at 7.00 (d, J=9.2Hz, 2H); 6.77 (d, J =9.6Hz, 1H) belongs to $H_{(j,k)}$ protons. The aliphatic region revealed a singlet peak along with a set of three singlet peaks belonging to $H_{(i)}$ protons, which appeared at 2.60 ppm. The spectra exhibited peaks at 2.51 and 3.37 ppm, corresponding to the DMSO-d_6 solvent and the amount of H_2O molecules in the solvent, respectively. **Figure 2** shows the ^{13}C NMR spectrum in DMSO-d_6, confirming the correct number of carbon atoms in the molecule. Resonances at δc=197.11 and 177.23 ppm were assigned to carbonyl carbon: (ketonic C_v); (iminic C_b), respectively. The Signal of phenolic carbon (C_p) was detected at 172.74 ppm. Resonances assigned for N- (C_n) were observed at 150.10 ppm, while the other N- (C_q) chemical shifts appeared at 147.06 ppm. The signals displayed at 138.92 ppm were related to (C_r). The peak related to (C_s) showed a frequency of 134.54 ppm, while the other two peaks, observed at 133.55 and 128.94 ppm, belong to carbon nuclei ($C_{x,w}$). The peak displayed at 127.46 ppm is attributed to (C_c). The four couples were assigned to groups of carbon nuclei ($C_{g,g-}$); ($C_{m,m-}$); ($C_{l,l-}$); ($C_{h,h-}$), at 127.34, 126.20, 125.72, and 124.57 ppm, respectively. Resonance of (C_j) signals appears at 122.82 ppm. The assignment of (C_k) resonance appeared at 122.31 ppm, while the resonance of (C_t) appeared at 121.63 ppm. The two carbon atoms ($C_{f,d}$) were observed at 121.25 and 117.70 ppm. The signal related to (C_u) was detected at 109.62 ppm. The methyl group (C_i) appeared as a single peak at 27.15 ppm, when the solvent signals of the DMSO-d_6 resonances appeared at 40.17 ppm[28–33].

4.2. Mass spectrum

The ligand mass spectrum was obtained by electron-scattering positive-ion mass spectrometry. The spectrum in **Figure 3** showed the presence of a parent ion $(M\text{-}H)^+$ at m/z=437.55amu (1%), corresponding to $C_{25}H_{18}N_4O_4$ (438.13amu), and signals above 437.55amu are impurities from the reaction. The fragmentation pattern for HL is illustrated in **Scheme 2**.

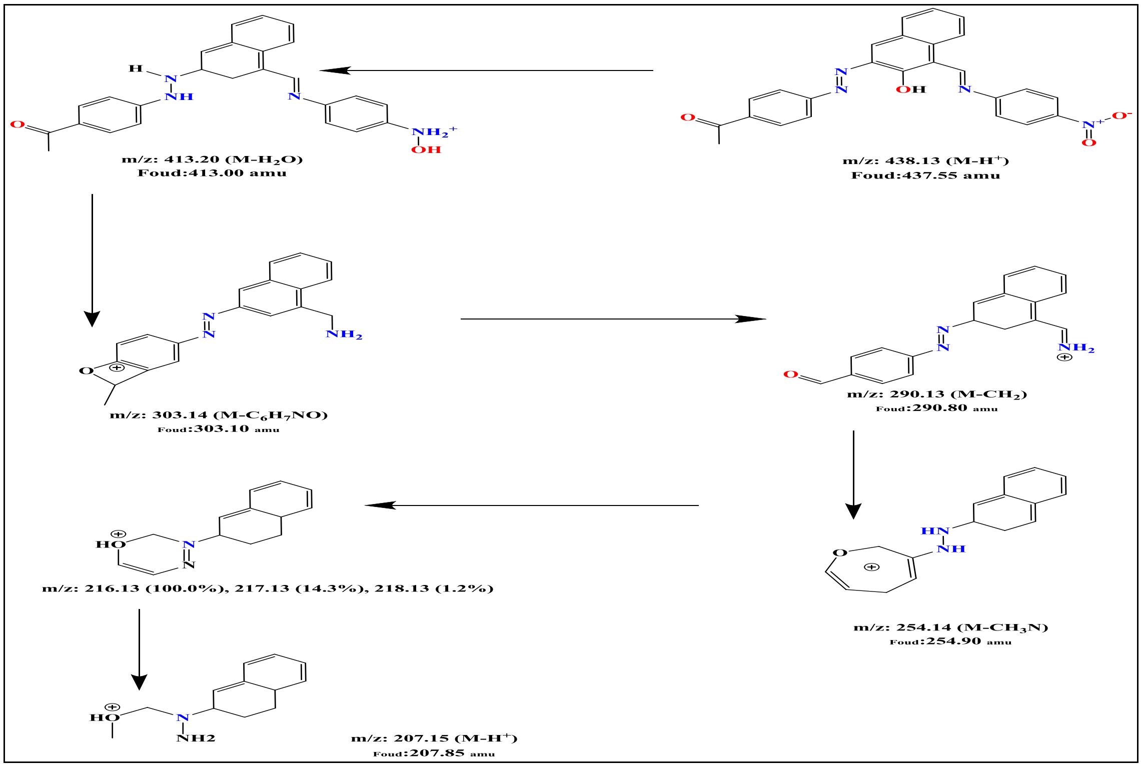

Scheme 2. The fragmentation pattern for HL

4.3. Electronic spectra and magnetic moment

Table 4 shows information on UV-visible spectra and magnetic moments. The electron spectrum of the complexes shows characteristic peaks between 257 and 298 nm, indicating transitions $\pi\rightarrow\pi^*$ and $n\rightarrow\pi^*$. Further, charge-transfer phenomena account for the observed peaks in an array between 314 and 481 nm[34,35]. For the spectrum of Cr (III), the band identified in the d–d region is displayed by a complex at 697 nm, which might be associated with $^4A_2g\rightarrow{}^2T_2g$, demonstrating a distorted octahedral configuration with the Cr (III). The magnetic moment of the Cr (III) ion, 3.80 BM, is consistent with this structural interpretation. Mn (II) complex spectra display the peaks that were discovered in the d–d region at 611 nm might be connected to $^6A_1g\rightarrow{}^4Eg(D)$, respectively. Electronic spectra of the Mn (II) complex confirmed a distorted octahedral geometry around the Mn (II) atom. Value of magnetic moment= 5.91 BM for ion Mn (II) is consistent with this structural interpretation. The spectrum of the Co (II) complex displays bands at 676 nm of the d-d region that correspond with the transition $^4A_2(F)\rightarrow{}^4T_1(p)$. The bands indicate a tetrahedral coordination environment around the Co (II) ion in a four-coordinate complex. Magnetic moment value of cobalt (II) ion= 4.64 BM, agrees with a tetrahedral arrangement around the Co ion[35, 36].

4.4. Thermal analysis

The study of the ligand's thermal decomposition was conducted in an argon (Ar) environment. The amount of weight was calculated from ambient temperature to 600°C. The thermogravimetric analysis results clearly indicated that the ligand decomposes in three stages, as shown in **Figure 4**. The weight loss in the 1st peak, observed at 173 °C in the thermogravimetric curve, can be attributed to the elimination of (CH_2) segments (obs.= 0.196 mg, 3.1%; cal.=0.197 mg, 3.1%). The 2nd step, observed at 173-305°C, could correspond to the loss of the ($CHO+CN+C_2N_2O$) segment (obs.= 1.73 mg, 28.07%; Cal.= 1.73 mg, 28.05%). The final step seen within 305-600°C may signify the loss of the ($CHO+C_2H_2+C_3H_2$) segment (obs.= 1.32 mg, 21.3%; calc.=1.31 mg, 21.2%). The remaining components of the ($C_{14}H_{10}NO$) segments (obs.= 2.93 mg, 47.4%; Cal.= 2.93 mg, 47.4%). The initial peak could be associated with the ligand's melting point[36,37]. The endothermic processes may be ascribed to the interaction of the organic ligand in an Ar environment. The thermal diagram of $[Cr(L)Cl(H_2O)_2]Cl$ complex was obtained in four steps, as shown in **Figure 5**. The 1st peak at 122°C may result from the loss of molecules from the (H_2O+CN+CO) segment; (obs.= 1.25 mg, 12.22%; calc.= 1.23 mg, 12.07%). The 2nd step occurred between 122 and 186°C, indicating the loss of the ($2CH_4$) segments (obs. = 0.548 mg, 5.35%; calc.= 0.549 mg, 5.36%). The 3rd step at 186-387°C is attached to the (C_2H_2+C_2N_2O) segment (obs.= 1.612 mg, 15.74%; calc.= 1.614 mg, 15.76%). The 4th step at 387-600°C is associated with (C_4H_2+CN) segment (obs.= 1.307 mg, 12.76%; calc.=1.305 mg, 12.74%). The remaining components of the (CrO+$C_{12}H_7C_{l2}O_2$) segments (obs.= 5.525 mg, 53.93%; calc.= 5.529 mg, 53.97%). The DTG exhibited several peaks at 52 and 210°C, indicative of an endothermic breakdown process. The endothermic processes may be ascribed to the interaction of the organic ligand in an Ar environment.

5. Conclusion

The Schiff base ligand (HL) and its paramagnetic complexes of metals involving chromium (III), manganese (II), and cobalt (II) have been reported. The ligand(HL) was synthesized from reaction of the 1-amino-4-nitrobenzene with ((E)-3-((4-acetylphenyl) diazenyl)-2-hydroxy-1-naphthaldehyde) in a one-to-one mole ratio. The interaction between ligands and metal ions at a (one-to-one) ligand-to-metal ratio generated isolated compounds, which have been structurally characterized via several physical and chemical techniques including elemental microanalysis, (^{1}H and ^{13}C) NMR, FTIR spectroscopy, electronic and mass spectroscopy, as well as magnetic susceptibility, conductivity measurements, and thermal analysis (TGA-DTG).

Acknowledgment

The authors express their gratitude to the Department of Chemistry, College of Education for Pure Science (Ibn Al-Haitham), University of Baghdad, for providing facilities for the MSc studentship.

Conflict of Interest

The authors declare that they have no conflicts of interest.

Funding

The funding section must include any financial support for the submitted work.

References

1. Sen T, Sarkar P, Sutradhar S, Das D, Ghosh BN. A review on platinum (II/IV) complexes of Schiff base ligands and application in biological activity. Inorg Chem Commun. 2024; 170(Part 3):113438. https://doi.org/10.1016/j.inoche.2024.113438.
2. Misganaw K, Thillairasu P, Shumi G, Debebe H, Berhanu S. Vanillin and 4-nitroanilline derived Schiff-base and its nickel (II) complex: spectral analysis and antibacterial investigation. Bull Chem Soc Ethiop. 2024; 38(5):1275-1289. https://doi.org/10.4314/bcse.v38i5.7.
3. Zhao P, Zhang X, Dong J, Li L, Meng X, Gao L. *In vitro* study of the pro-apoptotic mechanism of amino acid Schiff base copper complexes on anaplastic thyroid cancer. Eur J Pharm Sci. 2025; 206: 107005. https://doi.org/10.1016/j.ejps.2025.107005.
4. Yadav M, Yadav D, Singh DP, Kapoor JK. Macrocyclic Schiff base complexes of Zn (II), Cu (II), Co (II), and Ni (II) targeting topoisomerase IIβ: Synthesis, docking, and evaluation as potential anticancer agents. Appl Organomet Chem. 2025; 39(3):e7885. https://doi.org/10.1002/aoc.7885.
5. Kahraman S, Hepokur C, Erci F, Erkan S, Cetin S, Kose M, Kurtoglu M. Copper (II) complexes with N, O-donor azo-Schiff base ligands: Synthesis, structure, DFT studies, molecular docking, anticancer and antimicrobial activity. Polyhedron. 2025; 269:117393. https://doi.org/10.1016/j.poly.2025.117393.
6. Abd El-Lateef HM, Khalaf MM, Gouda M, Alharbi OA, Abdelhamid AA, Amer AA, Ismail AF, Abdou A. Fabrication, structural, DFT, biological and molecular docking studies of Fe (III), Ni (II),

and Cu (II) complexes based on Schiff-base derived from benzene-1, 4-diamine and 2-hydroxy-1-naphthaldehyde. J Indian Chem Soc. 2024; 101(2):101385. https://doi.org/10.1016/j.jics.2024.101385.

7. Ameen D, Hayyas S. Synthesis, characterization and antimicrobial evaluation of schiff base derived from sulfonamides and vanillin. Zanco J Med Sci. 2024; 28(1):9-18. https://doi.org/10.15218/zjms.2024.002
8. Kumar M, Singh AK, Gupta J, Singh S, Yadav RK, Singh AP. Exploring mixed-ligand cobalt (II) complexes with salicylaldehyde-based N, O-donor bidentate Schiff bases and neutral N-donor ligands: Synthesis, characterization, DFT, and antimicrobial studies. J Indian Chem Soc. 2025; 102(8):101803. https://doi.org/10.1016/j.jics.2025.101803.
9. Çakmak R, Başaran E, Şentürk M. Synthesis, characterization, and biological evaluation of some novel Schiff bases as potential metabolic enzyme inhibitors. Arch Pharm (Weinheim). 2022; 355(4):e2100430. https://doi.org/10.1002/ardp.202100430.
10. Ferretti V, Matos CP, Canelas C, Pessoa JC, Tomaz AI, Starosta R, Correia I, Leon IE. New ternary Fe (III)-8-hydroxyquinoline–reduced Schiff base complexes as selective anticancer drug candidates. J Inorg Biochem. 2022; 236:111961.https://doi.org/10.1016/j.jinorgbio.2022.111961.
11. Matos CP, Yildizhan Y, Adiguzel Z, Pavan FR, Campos DL, Pessoa JC, Ferreira LP, Tomaz AI, Correia I, Acilan C. New ternary iron (III) aminobisphenolate hydroxyquinoline complexes as potential therapeutic agents. Dalton Trans. 2019; 48(24):8702-8716. https://doi.org/10.1039/c9dt01193E.
12. Boublia A, Lebouachera SE, Haddaoui N, Guezzout Z, Ghriga MA, Hasanzadeh M, Benguerba Y, Drouiche N. State-of-the-art review on recent advances in polymer engineering: modeling and optimization through response surface methodology approach. Polym Bull. 2023; 80(6):5999-6031. https://doi.org/10.1007/s00289-022-04398-6.
13. Jarad AJ, Dahi MA, Al-Noor TH, El‑ajaily MM, AL-Ayash SR, Abdou A. Synthesis, spectral studies, DFT, biological evaluation, molecular docking and dyeing performance of 1-(4-((2-amino-5-methoxy) diazenyl) phenyl) ethanone complexes with some metallic ions. J Mol Struct. 2023; 1287(11):135703. https://doi.org/10.1016/j.molstruc.2023.135703.
14. Sakhare KB, Sakhare MA, Sarwade KN, Bharate YN. Synthesis, characterization, and anticancer, antidiabetic, and antimicrobial activities of azo-Schiff base ligand with ONO donor atom and its transition metal complexes. Anti-Infective Agents. 2024; 23(4). https://doi.org/10.2174/0122113525343891240925093331
15. Kargar H, Fallah-Mehrjardi M, Moghadam M, Zare-Mehrjardi HR, Omidvar A, Dege N, Acar E, Ashfaq M, Munawar KS, Tahir MN, Shahsavari HR. Tricoordinate copper (I) complexes of N,N-bidentate Schiff-base ligand: Syntheses, crystal structure determinations, electrochemical properties, theoretical studies, and catalytic activities. Inorg Chem Commun. 2025; 182:115512. https://doi.org/10.1016/j.inoche.2025.115512.
16. Mohan RD, Sarukrishna S, Babu AS, Santhosh D, Fathima SA, Parvathy B. A review of ligand denticity in copper–Schiff base complexes: Structural tuning toward enhanced antioxidant activity. Inorg Chim Acta. 2025; 590:122980. https://doi.org/10.1016/j.ica.2025.122980.
17. Mohammed HS, Tripathi VD. Medicinal applications of coordination complexes. IOP: Conference Series. 2020; 1664(1):012070. https://doi.org/ 10.1088/1742-6596/1664/1/012070.
18. Malav R, Sharma RK, Ray S. Versatile applications of cobalt and copper complexes of biopolymeric Schiff base ligands derived from chitosan. Int J Biol Macromol. 2026; 301:140338. https://doi.org/10.1016/j.ijbiomac.2025.140338.
19. Catalano A, Sinicropi MS, Iacopetta D, Ceramella J, Mariconda A, Rosano C, Scali E, Saturnino C, Longo P. A review on the advancements in the field of metal complexes with Schiff bases as antiproliferative agents. Appl Sci. 2021; 11(13):6027. https://doi.org/10.3390/app11136027.
20. Kumari P, Kumar A, Kataria R, Kaushik NK, Ahmed M, Ansari A, Ekta, Brahma M, Maruthi M, Babu YS, Singh B, Kumar V. Synthesis, characterization and biological studies of pyrazole-linked Schiff bases and their copper (ii) complexes as potential therapeutics. RSC Adv. 2025; 15(50):42299-42314. https://doi.org/10.1039/d5ra06008G.
21. Soroceanu A, Bargan A. Advanced and biomedical applications of Schiff-base ligands and their metal complexes: A review. Crystals. 2022; 12(10):1436. https://doi.org/10.3390/cryst12101436.

22. Abaas HJ, Al-Jeboori MJ. New dimeric complexes with semicarbazone mannish-based ligand; formation, structural investigation and biological activity. Revis Bionatura 2023; 8(2):15. https://doi.org/10.21931/RB/2023.08.02.15.
23. Behzad M, Ghasemi L, Capomolla SS. New Cu (II) complexes of unsymmetrical N_2O and N_2O_2 type Schiff base ligands: Molecular docking and pharmacophore modeling studies against a DNA duplex, Zika virus and Dengue fever proteases. Inorganica Chimica Acta. 2025; 583(6):122666. https://doi.org/10.1016/j.ica.2025.122666.
24. Hasan RH, Hasan HA. Synergism antibacterial activity for novel synthesized Schiff base ligands and semi-thiosemicarbazones with ß-diketones and 4-aminoantipyrine. Revis Bionatura 2022; 7(3):43. http://dx.doi.org/10.21931/RB/2022.07.03.43.
25. Mezher MQ, Yousif EI. New metal complexes with azo-Schiff base ligand synthesis, characterisation and biological activity. ICAIIT. 2025; 13(2):643-652. http://dx.doi.org/10.25673/120552.
26. Malav R, Ray S. Recent advances in the synthesis and versatile applications of transition metal complexes featuring Schiff base ligands. RSC Advances. 2025; 15(28):22889-22914. https://doi.org/10.1039/d5ra03626gG.
27. Ismail AA, Lateef SM. Synthesis a novel complexes of VO (II), Mn (II), Fe (II), Co (II), Ni (II), Cu (II) and Pt (IV) derived from Schiff's base of pyridoxal and 2-amino-4-nitrophenol and study their biological activates. IHJPAS. 2023; 36(2):259-275. https://doi.org/10.30526/36.2.3054.
28. Pasieczna-Patkowska S, Cichy M, Flieger J. Application of fourier transform infrared (FTIR) spectroscopy in characterization of green synthesized nanoparticles. Molecules. 2025; 30(3):684. https://doi.org/10.3390/molecules30030684.
29. Amjid Z, Khan S, Iqbal T, Hussain R, Ali HZ, Shoaib K, Khan Y, Ullah H, Arshad S, Iqbal R, Ullah R. Synthesis, confirmations and biological evaluation of acid substituted Schiff base Derivatives: Unraveling insight through SAR, DFT, ADMET and molecular docking. Results Chem. 2024; 11(21): 101744. https://doi.org/10.1016/j.rechem.2024.101744.
30. Abbas K, Zahid A, Parveen B, Amin I, Hussain S, Ahmed F, Munawar KS. Comprehensive investigation of organotin (IV) complexes derived from a novel Schiff Base: Synthesis, characterization, antioxidant, ADME profiling, and in vitro biological evaluation. Appl Organomet Chem. 2025; 39(1): e7761. https://doi.org/10.1002/aoc.7761.
31. Aazam ES, Majrashi M, Hussien MA. Exploring novel NH-form resorcinol-based Schiff base and its metal complexes: Synthesis, characterization, cytotoxic activity, molecular docking and ADME studies. Heliyon. 2024; 10(18):e37385.https://doi.org/10.1016/j.heliyon.2024.e37385.
32. Basaleh AS, Howsaui HB, Sharfalddin AA, Hussien MA. Substitution effect on new Schiff base ligand in complexation with some divalent Metal ion; synthesis, characterization, DFT and cytotoxicity studies. Results Chem. 2022; 4:100445. https://doi.org/10.1016/j.rechem.2022. 100445.
33. Kargar H, Abyar F, Zare-Mehrjardi HR, Fallah-Mehrjardi M, Munawar KS, Ashfaq M, Tahir MN. Indium (III) complex with NOON-tetradentate Schiff base ligand: Synthesis, crystal structure determination, electrochemical properties, theoretical studies, and molecular docking. Results Chem. 2025; 18:102909. https://doi.org/10.1016/j.rechem.2025.102909.
34. Khaleel HI, Al-Rubaye BK. New metal complexes derived from heterocyclic Schiff-base ligand; preparation, structural investigation and biological activity. IJDDT. 2022; 12(3):1341-1346. https://doi.org/10.25258/ijddt.12.3.68.
35. Anu D, Naveen P, Shyamsivappan S, Saravanan C, Arumugam N, Almansour AI, Frampton CS. New palladium (II) metallates containing ON donor Schiff base ligand. synthesis, spectral characterization, x-ray crystallography, photo physical and in vitro cytotoxicity. J Mol Struct. 2024; 1316:139000. https://doi.org/10.1016/j.molstruc.2024.139000.
36. Sogukomerogullari HG, Başaran E, Kepekçi RA, Türkmenoğlu B, Sarıoğlu AO, Köse M. Novel europium (III), terbium (III), and gadolinium (III) Schiff base complexes: Synthesis, structural, photoluminescence, antimicrobial, antioxidant, and molecular docking studies. Polyhedron. 2025; 265(1): 117275. https://doi.org/10.1016/j.poly.2024.117275.
37. Chen Q, Zeng MH, Wei LQ, Kurmoo M. A multifaceted cage cluster,[CoII6O12⊃ X]−(X= Cl− or F−): halide template effect and frustrated magnetism. Chem Mater. 2010; 22(14):4328-4334. https://doi.org/10.1021/cm1014459.